JACS
JOURNAL OF THE AMERICAN CHEMICAL SOCIETY
pubs.acs.org/JACS
Article

Impact of Low-Temperature Water Exposure and Removal on Zeolite HY

Anya Zornes, Nabihan B. Abdul Rahman, Omio Rani Das, Laura A. Gomez, Steven Crossley, Daniel E. Resasco, and Jeffery L. White*

Cite This: J. Am. Chem. Soc. 2024, 146, 1132−1143
Read Online
ACCESS | Metrics & More | Article Recommendations | Supporting Information

ABSTRACT: Aqueous-phase postsynthetic modifications of the industrially important Y-type zeolite are commonly used to change overall acid site concentrations, introduce stabilizing rare-earth cations, impart bifunctional character through metal cation exchange, and tailor the distribution of Brønsted and Lewis acid sites. Zeolite Y is known to undergo framework degradation in the presence of both vapor- and liquid-phase water at temperatures exceeding 100 °C, and rare-earth exchanged and stabilized HY catalysts are commonly used for fluidized catalytic cracking due to their increased hydrothermal resilience. Here, using detailed spectroscopy, crystallography, and flow-reactor experiments, we reveal unexpected decreases in Brønsted acid site (BAS) density for zeolite HY following exposure even to room-temperature liquid water. These data indicate that aqueous-phase ion-exchange procedures commonly used to modify zeolite Y are impacted by the liquid water and its removal, even when fractional heating rates and inert conditions much less severe than standard practice are used for catalyst dehydration. X-ray diffraction, thermogravimetric, and spectroscopic analyses reveal that the majority of framework degradation occurs during the removal of a strongly bound water fraction in HY, which does not form when NH_4Y is immersed in liquid water and which leads to reduced acidity in HY even when dehydration conditions much milder than those typically practiced are employed. Na^+-exchanged HY prepared via room-temperature aqueous dissolution demonstrates that Brønsted acid sites are lost in excess of the theoretical maximum that is possible from sodium titration. The structural impact of low-temperature aqueous-phase ion-exchange methods complicates the interpretation of subsequent data and likely explains the wide variation in reported acid site concentrations and catalytic activity of HY zeolites with high-Al content.

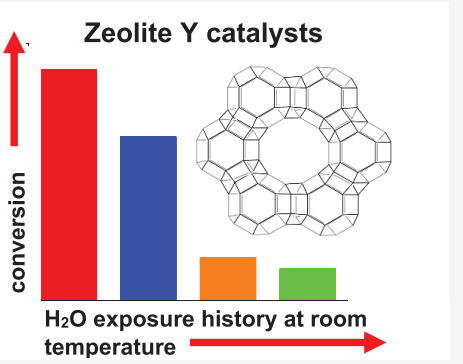

INTRODUCTION

Zeolites are an important class of materials that have been successfully implemented as commercial catalysts for gas-phase hydrocarbon conversion worldwide.[1−3] Interest in adapting zeolites for use with more complex feedstocks like biomass has increased dramatically in recent years, which requires zeolite exposure to liquid water at temperatures in excess of the boiling point of water.[4−7] Through extensive published literature and commercial practice, the stability of the acidic HY catalyst in the presence of water vapor and liquid water at elevated temperatures is now relatively well understood, with varying degrees of framework aluminum integrity arising from different zeolite framework structures and their respective channel topologies, Si/Al, hydrophilicity, acidity, defect density, and surface functionalizations.[8−14] Zeolite Y is the most widely used commercial zeolite catalyst industrially, with primary applications in fluidized catalytic cracking for which its high-temperature steaming stability in the presence of water vapor is improved through controlled dealumination and incorporation of rare-earth cations, yielding rare-earth exchanged ultrastable Y (USY or ReUSY) catalysts.[15−18] Zeolite Y stability is significantly lower in hot liquid water compared to steam at the same temperature, and previously, some of us have demonstrated routes to improved stability in hot liquid water using defect-free HY catalysts.[9] Recent studies have attempted to improve zeolite Y framework stability for hot liquid water-based chemistries and include surface hydrophobization and control of defect densities as viable modifications.[9,12,19−23]

The as-synthesized form of zeolite Y typically has a Si/Al ratio of 2.5−2.8, from which many other variants are derived via controlled dealumination, cation exchange, and surface functionalization through the silanol or bridging acid site groups. In addition, recent developments in methods to probe acid site proximity and paired sites in many zeolite catalysts including HY involve mono- or divalent cation titration from aqueous solutions of the catalyst, followed by spectroscopic

Received: November 7, 2023
Revised: December 4, 2023
Accepted: December 5, 2023
Published: December 29, 2023

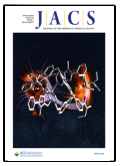

https://doi.org/10.1021/jacs.3c12437
J. Am. Chem. Soc. 2024, 146, 1132−1143

probes, typically either UV/vis or solid-state NMR, to measure the number or type of acid sites impacted by the titration.[24−26] Rare-earth and other metal cations are introduced for commercial applications, including targeted conversion and selectivity enhancements for protolytic cracking and hydrogen transfer reactions.[18,27−30] Also, the introduction of isotopically labeled water through a facile exchange process has been used to insert spectroscopically active nuclei into zeolite frameworks.[31−36] Inherent to all of the catalyst modifications listed above is the dispersal of the zeolite in excess liquid water at temperatures ranging from room temperature to ca. 80 °C for extended periods of time and then subsequent removal of water through dehydration methods in ambient air, flowing dry air or inert gases, or under vacuum.[27,28,36−40] In this contribution, detailed solid-state NMR spectroscopy, X-ray crystallography, and reactor experiments reveal that when zeolite HY with a Si/Al ratio of 2.6 is dispersed in liquid water at room temperature for relatively short exposure times, an irreversible loss of Brønsted acid sites (BAS) and concomitant framework Al occurs following even low-temperature and low-heating rate dehydration under inert vacuum conditions. Previously, it has been reported that octahedral framework Al sites in zeolite Y, whose formation is induced by ambient humidity, can undergo reversible transformation to tetrahedral framework coordination if the catalysts are subsequently treated with ammonia,[41−46] but the structural changes in HY caused by room-temperature liquid water exposure and removal are not facile. These unexpected findings help explain the widely varying values for BAS density in similar HY's reported in the literature and the fact that the measured BAS content in high-Al HY is usually significantly lower than the expectations based on Si/Al.[47−51] Results detailed here have significant implications for correctly interpreting results following postsynthetic ion-exchange methods commonly used to modify high-Al content HY.

EXPERIMENTAL SECTION

Catalyst Samples. Zeolite NH_4Y with a nominal Si/Al ratio of 2.6 (CBV300) was obtained from Zeolyst International. For NMR analyses, HY-2.6 was prepared from NH_4Y in a glass reactor by stepwise vacuum dehydration, heating at 0.5 °C/min to 120 °C, holding for 2 h, then heating at 2 °C/min to 450 °C, and holding for 12 h. A pressure of less than 1×10^{-4} Torr was maintained throughout using an Edwards EO4K diffusion pump.

Portions of these parent samples (NH_4Y-2.6, HY-2.6) were then dispersed in room temperature water, with a solid-to-liquid ratio of 250 mg to 10 mL, and stirred for 1 h. Catalysts were then vacuum-filtered and dried in a vacuum oven overnight at either room temperature or 80 °C. The liquid water-exposed NH_4Y sample deviated from this protocol in that it was immersed in liquid water at 70 °C for 6 h and was dried in atmospheric pressure and moisture at 80 °C. As a point of clarification, samples exposed to water are referred to by the form they were in during exposure, but all NMR characterization was done after converting to proton form. When mentioned, sample exposure to ambient humidity refers to laboratory relative humidity values of 50−55%.

Catalyst samples that were used in kinetic experiments were prepared by stepwise dehydration under 150 mL/min dried air, heating at 0.5 °C/min to 120 °C, holding for 2 h, then heating at 2 °C/min to 450 °C, and holding for 12 h.

Partial sodium exchange of HY-2.6 was conducted by stirring 200 mg of catalyst in 20 mL of 0.01 M $NaNO_3$ at room temperature for 1 h, followed by vacuum filtration and the same stepwise vacuum dehydration procedure as described above.

For convenience to the reader, Table 1 summarizes the key sample preparation steps in a simple nomenclature that facilitates the comparison of sample histories across the different experiments.

Table 1. Summary of the Naming Convention for Zeolite Y Samples vs Preparation and Thermal History[a]

notation	sample history
NH_4Y	commercial CBV300 sample as-received.
HY	CBV300 calcined (deammoniated and dehydrated) in vacuum (NMR) or under flowing dry air (reactor and TGA)
HY-LW	HY dispersed in excess liquid water at room temperature for 1 h prior to dehydration
HY-WLW	HY dispersed in excess liquid water at 70 °C for 1 h prior to dehydration
HY-CM	HY exposed to 99% humidity at 22 °C for 24 h and dried overnight at 80 °C in a vacuum oven
HY-AM	HY exposed to ambient humidity (50−52%) for 24 h and dried overnight at 80 °C in a vacuum oven

[a]Similar designations may be used for NH4Y samples, with the final tested form of all catalysts being the proton form. For example, NH4-LW indicates liquid water exposure while in the ammonium form but is always calcined prior to spectroscopic or reactor testing.

NMR Hardware and Sample Packing. NMR experiments on the dried solid catalysts were conducted at 9.4 T with a Bruker Avance II console using a 4 mm double-resonance MAS probe. Samples were packed in ZrO_2 rotors, under either ambient air or in an inert argon gas atmosphere, using a VAC atmosphere glovebox as necessary.

^{1}H NMR Experiments. ^{1}H NMR spectra were acquired using a single 5-μs excitation pulse. In all cases, 64 transients were collected by using a recycle delay of 60 s and a spinning speed of 10 kHz.

For quantitative spin-counting experiments, measured amounts of a vacuum-dehydrated sample and an inert internal standard poly(dimethylsiloxane) (PDMS) were packed in the middle third of an NMR rotor, with the bottom and top thirds filled by sulfur and a Teflon spacer, respectively. This ensures that the sample volume is within the homogeneous region of the excitation and detection coil. Using this method, the BAS and SiOH concentrations can be calculated.[52]

^{27}Al NMR. ^{27}Al single-pulse spectra were obtained with a 15° pulse of 0.58 μs, recycle delay of 0.2 s, and a spinning speed of 10 kHz for 2048 scans. Pulse durations and chemical shifts were calibrated by using a 0.1 M aqueous solution of $Al(NO_3)_3$.

^{29}Si NMR. ^{29}Si single-pulse spectra were obtained with a 90 pulse of 4.9 μs, recycle delay of 60 s, and spinning speed of 10 kHz for 1024 scans. Pulse durations and chemical shifts were determined using PDMS. Si/Al ratios were calculated from ^{29}Si NMR spectra using the equation $\frac{Si}{Al} = \frac{\sum Si}{Si(4Al) + \frac{3}{4}Si(3Al) + \frac{1}{2}Si(2Al) + \frac{1}{4}Si(1Al)}$ as each peak in the ^{29}Si spectrum corresponds to a Si near 0−4 Al atoms. However, the chemical shift of $(SiO_3)SiOH$, i.e., silanols, is the same as Si(1Al), which could artificially lower the Si/Al ratio of zeolites that contain a high number of SiOH due to framework hydrolysis.[53] Using the ^{1}H spin-counting method described above, the concentration of SiOH was calculated and compared to the total amount of Si present in the parent HY sample, as calculated from the IZA chemical formula. It was then determined what portion of the ^{29}Si signal should correspond to the SiOH species, and that portion of the signal was subtracted from Si(1Al). For higher Al zeolites, this change is negligible, but for hydrolyzed or dealuminated zeolites, this can drastically alter the Si/Al ratio.

XRD. Powder X-ray diffraction data were acquired at ambient humidity using a Phillips X-ray Diffractometer (Phillips PW 3710 MPD, PW2233/20 X-ray tube, copper tube detector, wavelength 1.5418 Å) operating at 45 kW, 40 mA. Diffractograms were obtained with 2θ ranging from 2 to 45° and a diffractometer difference of 0.02°.

Elemental Analyses and Ion-Exchange Capacity. Elemental analysis of Si/Al in HY and HY-LW catalysts was provided by

https://doi.org/10.1021/jacs.3c12437
J. Am. Chem. Soc. 2024, 146, 1132−1143

Galbraith Laboratories using the GLI ME-70 procedure. To determine the Na-ion exchange capacity for HY and HY-LW, each catalyst was exchanged with an aqueous 1 M $NaNO_3$ solution at room temperature, washed and dried at room temperature, and Na elemental analysis on the dried catalyst was completed by Galbraith Laboratories using the GLI ME-70 procedure.

Kinetic Measurements. The catalysts were used to convert *i*-octane in a continuous-flow microreactor at 400 °C under 80 mL/min flow of N_2. Before the reaction, the catalysts were pretreated to remove any latent moisture by heating at 0.5 °C/min to 300 °C, holding for 2 h, and then heating to reaction temperature at 2 °C/min. The reaction was carried out at 400 °C with 0.5 mL/h *i*-octane and 80 mL/min N_2 flowing over 50 mg of catalyst. The reaction conversion and product distribution were determined by a GC MS-FID system utilizing an HP-PLOT/Al_2O_3/"S" column.

Ammonia Temperature-Programmed Desorption (NH_3-TPD). The total acid site density was quantified using the temperature-programmed desorption of ammonia gas. Approximately 50 mg of catalyst was loaded in a continuous gas-phase reactor, and He gas was used as a carrier at a flow rate of 30 mL/min flow. The outflowing gas was connected to a MKS Cirrus mass spectrometer to track the m/z of 17, corresponding to ammonia. The catalyst was pretreated at 300 °C for 1 h to remove moisture. After the pretreatment, the temperature was cooled to 100 °C as a starting temperature, where the catalyst was saturated with a constant flow of 5 mol % NH_3 gas in He for 1 h. Then, physisorbed NH_3 was removed by keeping the temperature at 100 °C under He flow for 1 h. The catalyst, then, was heated to 650 °C at a 10 °C/min heating ramp. The NH_3 signal was calibrated for each run using 500 μL of 5 mol % NH_3 in He pulses.

Isopropyl Amine Temperature-Programmed Reaction/Desorption (IPA-TPD). Bronsted acid site density was quantified using a temperature-programmed reaction/desorption using isopropyl amine (IPA). Approximately 50 mg of catalyst was loaded in a continuous gas-phase reactor, and He gas was used as a carrier at 30 mL/min flow. The outflowing gas was connected to an MKS Cirrus mass spectrometer to track m/z of 17, 41, and 58, corresponding to ammonia, propylene, and IPA. The catalyst was pretreated at 300 °C for 1 h to remove moisture. After the pretreatment, the temperature was cooled to 100 °C as a starting temperature, where the catalyst was injected with several 2 μL IPA pulses until a consistent IPA area was detected by the mass-spectroscopy. After the pulses, the physisorbed IPA was removed by keeping the temperature at 100 °C under He flow for 1 h. The catalyst, then, was heated to 600 °C at a 10 °C/min heating ramp. From Hoffman's elimination, the propylene peak was used to determine the amount of total Bronsted acid sites. The propylene signal was calibrated for each run by using 500 μL of propylene pulses.

Thermogravimetric Analysis (TGA). The experiments were conducted using a NETZSCH STA Jupiter 449 F1 thermogravimetric analyzer (TGA) system with a constant flow of argon at 40 mL/min. The crucibles used for the analysis were made of Al_2O_3, and approximately 50 mg of each sample was used for the experiments. The samples underwent a consistent temperature ramp, with a heating rate of 2 °C/min from 30 up to 450 °C. For water and ammonia quantification, the samples were heated at a rate of 0.5 °C/min until reaching 120 °C and then held at this temperature for 2 h. Subsequently, the temperature was increased to 450 °C at a rate of 2 °C/min and maintained for 3 h. The evolving gases were analyzed by using a mass spectrometer (MKS Cirrus 2).

RESULTS AND DISCUSSION

The recent literature discusses the location of important rare-earth cations that stabilize the HY framework against framework hydrolysis during high-temperature steaming steps.[15,16,18,54] Other recent reports suggest that the small-pore sodalite units in HY can be accessed through strategic "opening up" of the caged subunits.[55,56] These reports demonstrate that there is still significant interest in understanding and extending the use of zeolite HY to many new applications, as well as optimizing their use for increased selectivity in known gas-phase hydrocarbon chemistries. Many HY applications involve postsynthetic ion exchange in aqueous salt solutions to introduce rare-earth cations, probe the acid site location and proximity with mono- and divalent probe cations, and impart new functionality through metal intercalation, hydrophobization, or other specific chemical modifications.[21−27,55−58] While many of these chemistries begin with the NaY or NH_4Y form, some begin with the acidic HY catalyst, particularly those in which the goal is to interrogate the Brønsted acid site location and paired acid site proximities, as well as modify acid site densities via partial cation exchanges or selectively "poisoning" very strong acid sites. In all cases, zeolite crystallites are suspended in excess liquid water at 25−80 °C for extended time periods. Often, the process is repeated multiple times to prepare a single ion-exchanged catalyst. Based on the difficulty encountered in reproducing some rare-earth exchanged HY (REHY) data, as well as larger reported discrepancies between measured acid site content and framework Al content in HY relative to many other zeolites,[59−62] a systematic investigation of the impact of excess liquid water and its removal on zeolite HY under the low-temperature conditions representative of typical ion-exchange conditions was warranted.

In early work, Kerr noted that the ion-exchange capacity of zeolite HY was significantly reduced following liquid water immersion for 10 to 15 s at room temperature, attributing the result to a combination of reversible and irreversible hydrolysis of the framework at Al atom sites.[63] Subsequently, Parker et al. stated that "zeolite HY, formed by heating NH_4Y, is unstable and hydrolyzes rapidly in water with the loss of structural aluminum."[64] In a very recent contribution, Heard and co-workers stated that "under ambient conditions, aluminosilicate zeolites are stable when exposed to water or water vapor" but discussed how hot liquid water and steaming can lead to structure degradation in aluminosilicates as well as the water-induced manipulation of germanosilicate structures through the assembly disassembly organization−reassembly (ADOR) process.[65] In the interim, between these apparently conflicting reports, excess liquid water has routinely been used as the solvent for modifying Y-type zeolites via ion-exchange procedures at temperatures ranging from room temperature to ca. 80 °C.[57,66−79] While most procedures involve starting with the NaY or NH_4Y form of the zeolite, the latter of which affords significant protection against deleterious water effects as indicated by the data in Figure 1 (vide infra), many begin with the HY form.

Impact of Water on the Catalyst Structure. Based on the confusion surrounding low-temperature water's impact on zeolite HY, and in an effort to clarify whether it is primarily the water exposure or water removal steps that potentially impact the catalyst structure, a series of HY samples were investigated following various water exposure and drying steps. Figure 1 shows the ^{1}H MAS NMR spectra of dehydrated HY catalysts following preparation with and without exposure to room-temperature liquid water. With no exposure to liquid water, HY lacks any significant SiOH signal and has a BAS concentration relatively close to the theoretical maximum value of 4.2 mmol/g, as shown by the intense signals arising from the BAS proton in the supercage (3.9 ppm) and the sodalite cages (4.9 ppm) in Figure 1a. Figure 1b shows that similar acid site concentrations are obtained if the catalyst was

https://doi.org/10.1021/jacs.3c12437
J. Am. Chem. Soc. 2024, 146, 1132−1143

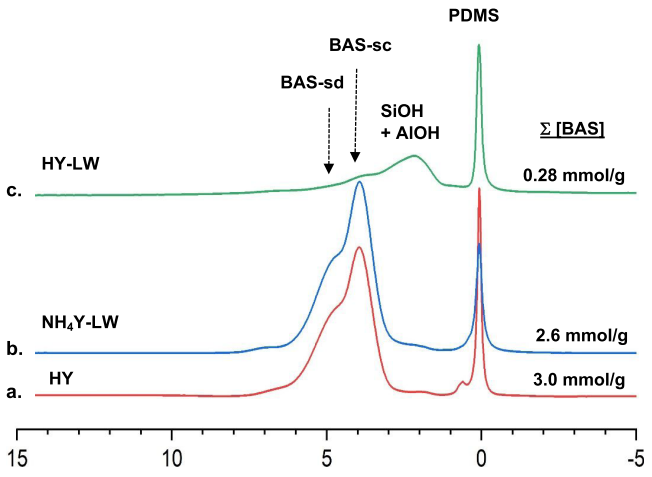

Figure 1. ^{1}H MAS NMR spectra of dry zeolite: (a) HY, i.e., prepared from NH_4Y following low-ramp-rate stepwise vacuum dehydration up to 450 °C; (b) NH_4-LW, i.e., prepared from NH_4Y dispersed in excess liquid water at 70 °C for 6 h prior to same dehydration procedure as in panel (a) to yield the HY form of the catalyst; (c) HY-LW, i.e., prepared from HY dispersed in excess liquid water at room temperature for 1 h prior to same dehydration procedure as in panel (a). Total concentrations of BASs from both sodalite (BAS-sd) and supercage (BAS-sc) locations are listed at right. The 0 ppm peak arises from the poly(dimethylsiloxane) (PDMS) internal quantitation standard. All spectra were acquired at 10 kHz rotor spinning speeds. Note the absence of significant silanol (SiOH) signals in parts (a) and (b).

immersed in liquid water at 70 °C while in the ammonium form (NH_4Y) for several hours and converted to proton form following the same vacuum dehydration procedure used for the catalyst in 1a. Surprisingly, if the acidic zeolite HY is exposed to liquid water *at* 25 °C for only 1 h, substantial SiOH signals at 2 ppm along with a poorly resolved nonframework AlOH contribution near 3 ppm[13] are observed with a concomitant 10-fold reduction in BAS concentration as demonstrated by the spectrum in Figure 1c. The spectra in Figure 1 are acquired under quantitative conditions with the 60 s delays between accumulated transients exceeding five times the longest relaxation time T_1, and the addition of known amounts of inert PDMS (poly(dimethysiloxane)) provides a convenient internal calibration standard against which all signals can be quantified. Complete experimental details for quantitative spin-counting in dehydrated zeolite catalysts have been reported previously.[59] Example deconvoluted spectra for Figure 1 using mixed Lorentzian−Gaussian line shape components are shown in Figure S1 and reproducibility and uncertainty were addressed by running 15 NMR experiments on 7 different samples like the starting catalyst shown in Figure 1a, with a mean [BAS] equal to 3.0 mmol/g and one standard deviation equal to 0.68 mmol/g. This standard deviation determined for HY is 1 order of magnitude larger than previous results obtained for the MFI catalyst HZSM-5 using identical experimental protocols,[25,52] reflective of the increased moisture-sensitivity of its high-Al content structure (vide infra). For HY samples exposed to liquid water and dried, e.g., like that shown in Figure 1c, the standard deviation reduced to 0.1 mmol/g.

To clarify whether any residual water impacted the interpretation of the vacuum-dehydrated spectra in Figure 1, as recently discussed in the literature using controlled water-addition experiments in the medium-pore MFI zeolite,[80,81] deconvolution and spin-counting analysis of all peaks downfield of the BAS peaks in Figure 1a−c were completed. For the HY-LW spectrum in Figure 1c, the maximum possible residual water amount in that catalyst based on assigning all peaks in the ≥6 ppm region of the chemical shift scale to residual water in the dried catalyst is 0.007 mmol/g or 0.02 water/Al. The only measurable signals that could possibly be assigned to residual water were in the 6−7 ppm region, not in the 7−9 ppm region as has been assigned to hydroxonium ions for the medium-pore HZSM-5 zeolite.[81] More likely, the HY catalysts studied here exhibit weak signals in the 6−7 ppm region due to residual ammonium species, as the intensity of the same signals in Figure 1b for the NH_4Y-LW sample corresponds to 0.03 mmol/g, much greater than that in HY-LW. This result is consistent with the above peak assignment since the HY-LW has been vacuum dehydrated twice and thus is more likely to remove any residual ammonia versus only once for NH_4Y-LW. Thus, within the confidence limits of the experiment, no residual water contributions to the spectra of the vacuum-dehydrated samples were detected.

Figure 2 shows the ^{27}Al MAS NMR spectra of the same series of samples as in Figure 1, including as-received and

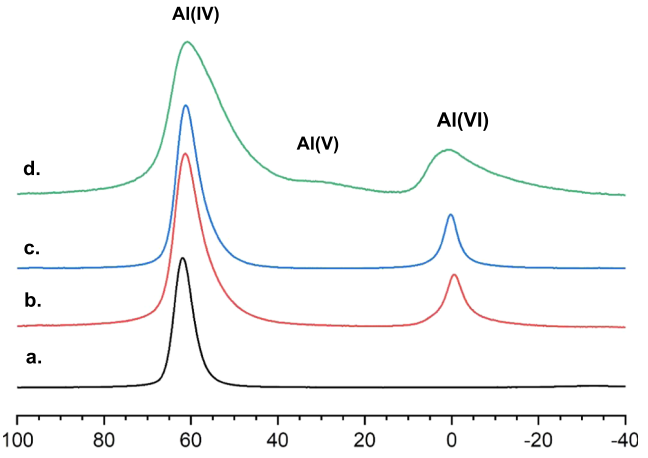

Figure 2. ^{27}Al MAS NMR spectra acquired at ambient hydration of (a) NH_4Y; (b) HY, i.e., same sample as in Figure 1a but after exposure to ambient moisture to facilitate spectral acquisition in the absence of ^{27}Al quadrupole broadening; (c) NH_4-LW, i.e., same as in Figure 1b but after exposure to ambient moisture; and (d) HY-LW, i.e., same as in Figure 1c but after exposure to ambient moisture. Spectra are scaled to the height of the largest peak; to compare stack plots of all spectra on the same scale, see Figure S2.

unheated NH_4Y as a control, with spectra acquired for catalysts exposed to ambient atmospheric moisture. To note, the spectra in Figure 2 are each normalized to the height of the largest peak for clarity, but Figure S2 shows the spectra plotted on the same intensity scale. As expected, NH_4Y is entirely stable in ambient air (Figure 2a) with respect to the preservation of tetrahedrally coordinated framework Al, as indicated by the signal at 60 ppm. Figures 2b and 2c compare two HY catalysts prepared from NH_4Y, without (Figure 2b) and with (Figure 2c) dissolution of the NH_4Y in liquid water, directly comparable to the samples in Figure 1a,1b, with a new peak at 0 ppm arising from hexacoordinated nonframework Al sites now clearly visible in both. Again, the catalysts in Figure 2b,c were exposed to the same low-ramp rate stepwise vacuum heating procedure used to acquire the ^{1}H spectra of completely

https://doi.org/10.1021/jacs.3c12437
J. Am. Chem. Soc. 2024, 146, 1132−1143

dehydrated samples in Figure 1, but following exposure to ambient moisture. Finally, Figure 2d shows the ^{27}Al MAS NMR spectrum acquired for an initial HY catalyst subjected to liquid water exposure similar to that used to acquire the spectrum in Figure 2c, but for only 1 h of water dissolution at 25 °C instead of the 6 h and 70 °C used for the starting NH_4Y in 2c. Again, Figures 1b and 2c are from the same sample type and history as Figures 1c and 2d. Figures 2d and S2a−d clearly show that when HY is exposed to liquid water at room temperature and that water is then removed using an extremely mild vacuum dehydration protocol, there is a significant loss of framework tetrahedral Al and creation of both penta- and hexacoordinated Al species, completely consistent with the large decrease in BAS concentration shown in Figure 1c.

Figure 3 shows ^{29}Si MAS NMR spectra of the same samples as in Figure 2, with calculated Si/Al ratios to the right of the spectra. Using the same peak assignments as in the other spectra, the calculated Si/Al ratio for HY after exposure to liquid water would be 4.0, which would not only give an expected BAS content ten times higher than the observed amount from ^{1}H experiments but is also inconsistent with the ^{27}Al data in Figure 3c,3d. X-ray diffraction data shown in Figure S3 show that crystallinity is reduced to 59% after only 1 h exposure of HY in liquid water at 25 °C and then dehydration, i.e., for the samples in Figures 1c, 2d, and 3d. Clearly, there is significant amorphous content increasing T−O−T bond angle heterogeneity as seen by the broadening of all ^{29}Si signals in 3d, and indeed, this spectrum is similar to literature spectra from amorphous silica−alumina.[82−85] These broad and overlapping signals complicate the deconvolution of the spectrum, causing the standard calculation to underestimate the Si/Al ratio.

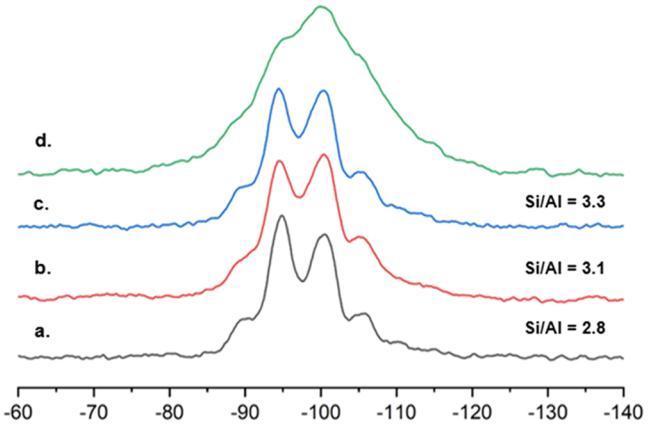

Figure 3. ^{29}Si MAS NMR spectra acquired at ambient hydration of (a) NH_4Y; (b) HY, i.e., the same sample as in Figure 1a; (c) NH_4Y-LW, i.e., the same sample as in Figure 1b; and (d) HY-LW, i.e., the same sample as in Figure 1c. Si/Al ratios determined via deconvolution of the ^{29}Si spectra are listed at right.

In order to define the final Si/Al of the HY-LW catalysts, elemental analysis obtained via ICP-AES shows that the overall Si:Al of 2.6:1 is unchanged relative to the starting HY. This result is expected since XRD, NMR, and TGA-MS (vide infra) indicate that the majority of structural damage yielding the amorphous nonframework components does not occur while in liquid water but when removing adsorbed water in the subsequent elevated-temperature dehydration steps. As such, there is no liquid water phase by which the generated nonframework Al can be removed from the zeolite interior and remains as detrital Al moieties within the zeolite pores.

Impact of Water on Catalyst Performance. The impact of room-temperature liquid water exposure and its removal on catalyst conversion was evaluated using isooctane cracking reactions at 400 °C. Figure 4a shows that a ca. 7-fold decrease in isooctane conversion per unit catalyst mass occurs for an HY catalyst that was dispersed in liquid water and then dehydrated (red vs green bar), completely consistent with the reduced [BAS] calculated from the NMR spectra in Figure 1. Figure 4a also demonstrates that HY exposure to sources of vapor-phase water, either as ambient ca. 50% humidity (blue bar) or controlled 99%-humidity (orange bar), can have relatively minor to relatively major impacts on catalyst performance. The origin and implications of these changes in catalyst performance based on the details of a catalyst's water history, as well as supporting spectroscopy data, will be discussed in more detail

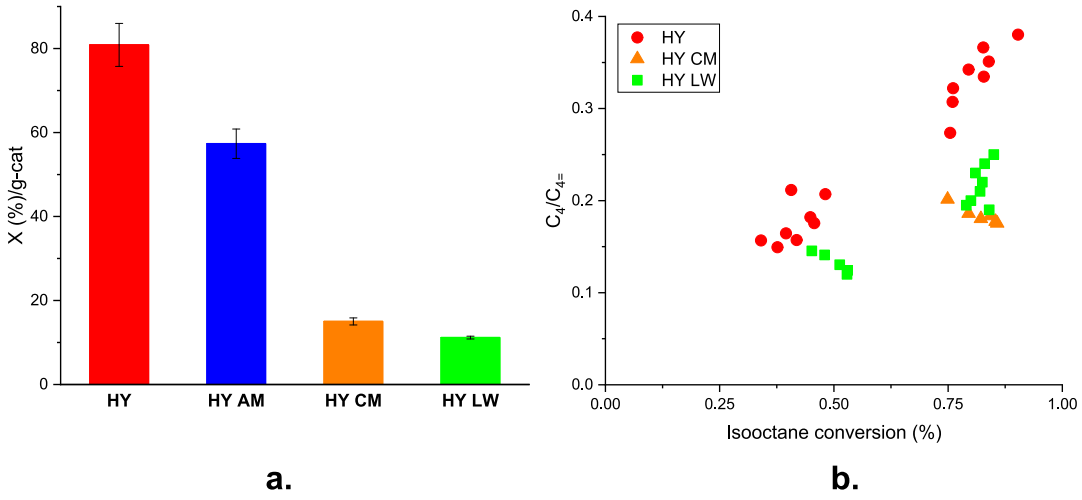

Figure 4. (a) Isooctane (2,2,4-trimethylpentane) conversion per gram of catalyst mass in the flow reactor using HY prepared from NH_4Y according to the calcination treatment in the Experimental Section, compared to that for HY exposed to different vapor- or liquid-phase water treatments as noted. Error bars reflect the deviation in activity over 225 min time on stream. (b) $C_4/C_4^=$ (predominately isoalkane to isoalkene) ratio vs isooctane conversion, demonstrating that selectivity is also impacted by water exposure and removal.

https://doi.org/10.1021/jacs.3c12437
J. Am. Chem. Soc. 2024, 146, 1132−1143

below. The catalyst activity for all catalysts is relatively stable (Figure S4), and the products formed are primarily methane, propene, butane, and butene (Table S1). To clarify, this work operates at lower conversions, higher temperatures, and lower reactant partial pressures and thus obtained simpler product distributions than those previously reported.[86,87] Figure 4b shows the $C_4/C_4^=$ (primarily isobutane/isobutene) ratio as a function of isooctane conversion in HY before and after exposure to excess humidity or to liquid water, revealing a significant change in the isobutane:isobutene product ratio. This change could originate from the decreased acid site density and proximity in the water-exposed catalyst, reducing secondary oligomerization and cracking reactions involving isobutene. We note, however, that other surface features that modify the local environment surrounding active sites, e.g., site proximity, presence of EFAl, and partially coordinated framework species, have been demonstrated to parallel changes in catalyst reactivity.[25,26,60,88] As suggested by the spectroscopy results in Figures 1−3, the reaction data in Figure 4 unequivocally demonstrate that any aqueous-phase ion-exchange steps involving HY impart significant changes to conversion and selectivity independent of the amount or type of cation used. As discussed below, care must be exercised in attributing such changes to the action of specific cations in the zeolite, as they could simply result from the water effects demonstrated here.

As an example of a typical ion-exchange procedure that might be used to modify acid sites in HY, Na^+ exchange experiments were used to partially titrate BASs. A partial exchange using substoichiometric amounts of Na^+ was attempted to determine if BASs in sodalite cages or supercages were preferentially titrated, as this is an open question in the catalytic literature regarding HY.[56,76−78] Figure 5 shows ^{1}H MAS NMR of dry HY before and after Na titration with a 0.25

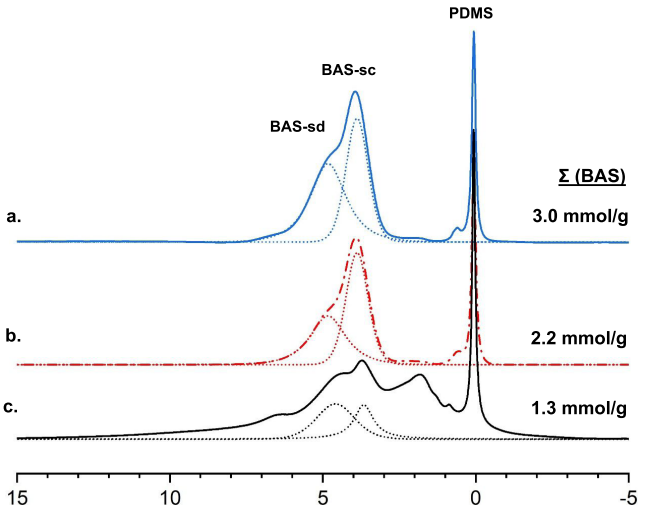

Figure 5. ^{1}H MAS NMR spectra of dry zeolite Y (a) prepared from NH_4Y following low-ramp-rate stepwise vacuum dehydration up to 450 °C, i.e., same sample as in Figure 1a; (b) calculated from HY with 75% of original BAS concentration, i.e., the expected spectrum after titration with 0.25 Na:Al loading; (c) prepared from HY titrated with 0.25 Na:Al loading in excess liquid water at room temperature for 1 h prior to same dehydration procedure as in (a). Total concentrations of BASs are listed on the right, with (a) and (c) being experimental and (b) being theoretical. The 0 ppm peak arises from the poly(dimethylsiloxane) (PDMS) internal quantitation standard.

Na:Al molar ratio. Not only does the 0.25-NaY spectrum contain much higher amounts of SiOH groups reflecting the destruction of the catalyst framework, but the total BAS concentration is only 1.3 mmol/g (43% of HY's 3.0 mmol/g) rather than the 2.2 mmol/g that would be expected as a theoretical minimum assuming complete Na^+ exchange. Given the extremely mild exchange conditions, studies utilizing aqueous-phase cation exchanges must be careful to account for the instability of high-Al HY's to liquid water and its removal. For example, if a divalent cation had been used in this case as a probe for proximate or synergistic acid sites, the results would likely be incorrectly interpreted as acid site loss resulting from the cation effect only.

Relative Impact on Sodalite vs Supercage Acid Sites. The data in Figures 1 and S1 suggest that the relative impact of low-temperature liquid water exposure and removal is more significant for BASs in the sodalite unit than in the supercage of HY. Figure S1a shows that prior to any liquid water exposure, the BAS_{sod}:BAS_{sup} ratio is greater than 1. Figure S1b indicates that following immersion in room-temperature liquid water for one h and water removal, that same ratio decreases to ca. 0.5. Recent reports discuss several novel approaches to making the BASs in sodalite units more accessible using fluoride etching agents.[54,55] The results presented in Figures 1 and S1 suggest that alternative routes to fluoride reagents based strictly on liquid water dissolution and removal might exist and are being explored for future applications.

Alternative HY Dehydration Methods. The spectroscopy and reaction data discussed above suggest that the amount of water left in HY prior to dehydration is the likely major contributor to the loss of BASs in HY with a high Si/Al. XRD results in Figure S3c,d show that when the HY catalyst is only exposed to liquid water but not dehydrated using the standard heating protocols commonly employed in zeolite applications, there is only a small (5%) crystallinity loss. Also, Figure S3a vs S3c shows that exposing the NH_4Y form of the zeolite to the liquid water results in a similar small loss in crystallinity of 4%. Thus, the impact of liquid water on the catalyst structure, in either the ammonium or protium form, is similar. However, a comparison of Figures S3c to S3d and S3e demonstrates that the water removal step in HY leads to significant crystallinity losses, e.g., a 25% decrease relative to a similarly prepared HY catalyst that has not been exposed to liquid water.

In an effort to remove as much water as possible prior to the vacuum dehydration heating protocol, some HY catalysts exposed to liquid water were kept in a vacuum oven at room temperature for several days prior to the heating protocol described in the Experimental Section. Even so, the [BAS], tetrahedral framework Al, and crystallinity all decreased as discussed above. In further attempts to remove as much water prior to reaching elevated temperatures in the vacuum dehydration program, 0.1 °C and 0.5 °C/min heating ramp rates were used in concert with extended 12−24 h hold times at temperatures ranging from 80 to 200 °C, and in various combinations, but with similar negative impacts on HY acid site density as shown by the spectra in Figure S5. In all cases, the original [BAS] of about 3 mmol/g decreased at least 7−10-fold.

Origin of Water's Impact on the Structure and Acidity in HY. The XRD and NMR data discussed above indicate that while there was a 4% decrease in crystallinity following immersion in liquid water, the majority of structure impact resulted from water removal. To further elucidate how

https://doi.org/10.1021/jacs.3c12437
J. Am. Chem. Soc. 2024, 146, 1132−1143

Table 2. Summary of BAS and LAS Concentrations and Corresponding Reaction Data for Catalysts as a Function of Liquid Water or Moisture Exposure History

samples	total acid[a] (BAS + LAS) (mmol/g_{cat})	total BAS[b] (mmol/g_{cat})	supercage BAS[b] (mmol/g_{cat})	IPA-TPD BAS (mmol/g_{cat})	LAS[c] (mmol/g_{cat})	isooctane cracking reaction[d]	
						X (%)/g-cat	TOF[e] (h^{-1})
HY	2.23	3.0	1.40	1.10	1.13	80.9	2.22
HY-AM		3.0[f]				57.3	
HY-CM		0.39				15.0	
HY-LW	1.51	0.28	0.19	0.25	1.26	11.2	1.27

[a]NH_3 TPD [b]Quantitative ^{1}H NMR data [c]Difference between total acid and IPA-TPD BAS [d]Reaction conditions: 50 mg cat, 2.74 kPa iC8 partial pressure, flow mode, 400 °C, 80 mL/min N_2 carrier. Pretreatment: 0.5 °C/min to 300 °C and hold 2 h. Heat to 400 °C at 2 °C/min [e]Calculated using BAS from IPA-TPD [f]Not the same "HY+ambient" sample as used for the isooctane cracking reaction; prepared via vacuum dehydration for NMR vs air-drying in the final dehydration step of the reactor experiment

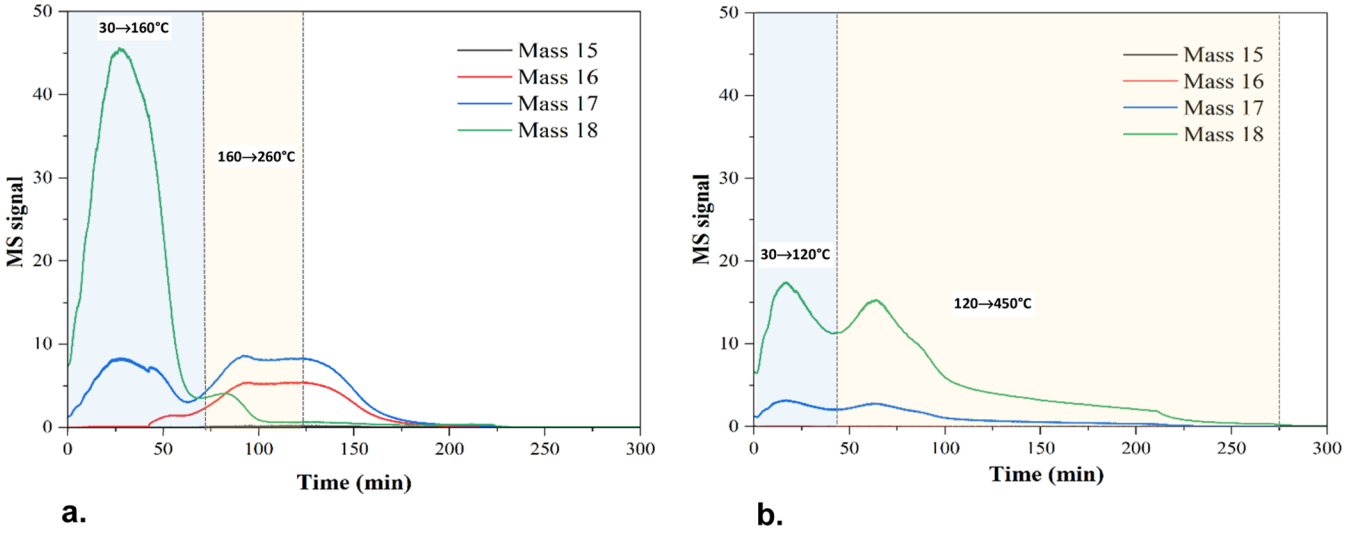

Figure 6. Mass signal intensities following thermal desorption and mass detection of water and ammonia as well as their fragments from (a) NH_4Y-LW, showing both significant ammonia (primarily mass-17) and water (mass-18) desorption and (b) HY-LW. The temperature ranges corresponding to water desorption times are indicated by the demarcation lines and associated text. Note the significant differences in the amounts and desorption behavior of the two water populations observed in NH_4Y (a) vs HY (b) given by the green mass-18 trace. Ammonia and water fragments can also contribute to mass-16 and mass-17 intensity, respectively, but the ammonia fragment NH_2^- exclusively contributes to mass-16 in NH_4Y (a) and OH^- exclusively to mass-17 in HY (b).

water exposure at low temperatures ultimately leads to these deleterious structural impacts and the significantly reduced isooctane conversions in Figure 4, a series of additional controlled water exposure and removal methods were conducted.

First, spectroscopy experiments following exposure of dehydrated HY to ambient moisture, i.e., ca. 50% relative humidity for 48 h, reveal that ambient moisture at that humidity level does not lead to any significant loss of BASs. Figure S6 shows similar data to that previously discussed in Figure 1, in which it can be observed that the total number of BASs in the ^{1}H NMR spectrum, as well as their distribution in sodalite vs supercage locations, does not change after exposing dehydrated HY to ambient moisture for 2 days. Figure S6 also indicates that the removal of that ambient moisture through controlled vacuum dehydration does not negatively impact the HY structure. These data suggest that structural degradation occurs only when the amount of water inside the catalyst at the time of its removal exceeds that which is encountered in typical ambient laboratory conditions. In Figure 4a, the blue bar shows that conversion results for a similar HY sample exposed to ambient humidity do lead to a relatively small decrease in conversion, but it should be noted that the sample used there was dehydrated prior to reaction in dry air, whereas the sample used to obtain the spectrum in Figure S6 was dehydrated on a high-vacuum line. What is clear from the spectral data in Figure 1 and S6, as well as the reactor data in Figure 4, is that the HY structure and activity impacts from ambient vapor-phase water are minimal compared to that imparted by liquid-phase water. It is possible that ambient moisture exposure for periods of time much longer than those investigated here can have significant impacts on framework integrity, but that was outside of the scope of this work.

Second, HY zeolites were exposed to controlled moisture environments using the experimental apparatus shown in Figure S7. Samples were placed in sealed containers at 22 °C with an internal moisture level equal to 99% relative humidity for 24 h. Following dehydration using the standard calcination procedure described in the Experimental Section, these "controlled moisture" HY samples were tested for isooctane cracking, as shown by the orange bar and data points in Figures 4a and 4b, respectively. The 15% isooctane conversion using the moisturized-HY catalyst was low compared to the HY control sample at 80% and only slightly higher than the ca.

https://doi.org/10.1021/jacs.3c12437
J. Am. Chem. Soc. 2024, 146, 1132−1143

10−12% obtained for the HY catalyst exposed to liquid water. The slightly higher conversion for the controlled moisture sample compared to the liquid water sample agrees with the slightly higher [BAS] of 0.39 vs 0.28 mmol/g, respectively, as measured by the quantitative ^{1}H spin-counting NMR experiment. While not shown, the spectrum for the controlled moisture HY was in every way consistent with that shown in Figure 1c for the liquid water treated sample. Table 2 summarizes acid site concentrations and reaction data for HY catalysts as a function of water exposure history, with all data consistently supporting the significant loss of BASs in HY-LW. Further, and consistent with these data, the Na-ion exchange capacity as measured by elemental analysis of the room-temperature Na-exchanged HY-LW is only 1.99 wt %, a significant reduction from the 6.03 wt % measured for the starting HY catalyst.

Finally, quantitative desorption experiments were used to investigate the temperature range and mass loss associated with water and ammonia removal based on the water exposure history of HY catalysts. Experiments on the parent NH_4Y catalysts were conducted in parallel for reference. Comparisons between standard differential thermocouple detectors and mass spectrometer detection were used to verify assignments. Figure 6 shows thermal desorption-mass detection data for NH_4Y (Figure 6a) and HY (Figure 6b) catalysts exposed to liquid water, with data acquired using the 2 °C/min heating ramp shown in Figure S8. After liquid water immersion and prior to the thermal desorption data collection, each catalyst was dried in a vacuum oven at 80 °C overnight. The mass-16 and longer-time mass-17 traces in 6a confirm that relatively high temperatures are required to completely remove NH_3 from the catalyst, as expected. While NH_3 is the primary contributor to the mass-17 response, the water fragment OH^- can also contribute, which accounts for the additional short-time feature in the blue trace in 4a, mirroring the mass-18 response. Mass-18 arises exclusively from water, and the ammonia fragment NH_2^- is the only contribution to mass-16.

Comparing the mass-18 time and temperature evolution in Figure 6a vs 6b, it is clear that both two populations of water are observed evolving at low and high temperatures. In HY, the majority of the water desorbs in a relatively high-temperature region, whereas in NH_4Y, most of the water desorbs at low temperatures. Indeed, quantitative analysis of the desorption data in 6a indicates that almost 90% of all water in the NH_4Y sample is removed by ca. 150 °C. In HY, more than 50% of the total water remaining in the catalyst exists in the high-temperature desorption population, requiring temperatures in excess of 400 °C to ultimately remove. These data indicate that following liquid water exposure in HY, ca. 50% of the remaining water exists as "strongly bound" water during the dehydration steps, which, according to the spectroscopy data in Figures 1−3 and reactor data in Figure 4, leads to significant framework hydrolysis. Only ca. 10% of all adsorbed water forms a strongly bound water population in the NH_4Y catalyst due to the stoichiometric complexes between the ammonium cation and the framework Al sites, thereby preventing irreversible framework degradation. While framework healing functions of ammonia in Y-type catalysts have been reported,[43−45] the significant framework destruction for HY in the presence of water under the very mild conditions routinely used for catalyst modifications in aqueous solutions is not widely known. Additionally, Figure 6 suggests that some fraction of those water molecules in the high-temperature desorption require more energy to desorb than ammonia molecules, corresponding to the time axis points greater than 175 min in Figure 6b. Detailed information on the quantitative analysis of water and ammonia desorption can be found in Figure S9.

Synopsis of Water Attack Mechanisms. Several experimental and computational investigations for hydrolysis of framework Al sites in zeolites, including FAU-type zeolites, have recently been published.[89−92] As discussed above, while some slight degradation of zeolite crystallinity occurs while the HY is in liquid water, the majority of crystallinity loss and concomitant reduction in acidity occur during water removal steps. This is consistent with several recent reports. First, Ashbrook and co-workers have shown that facile exchange of oxygen atoms around framework sites occurs at room temperature, with lower barriers to bond breaking at Al−O sites compared to Si−O sites, but that overall structure is preserved.[31,34] With the addition of the necessary thermal energy required for bond breaking and rearrangement of species, framework extraction of solvated tetrahedral atoms is believed to occur. While important contributions have appeared in the literature detailing the barriers associated with sequential water addition in FAU zeolites leading to dealumination, thereby revealing lowest-energy attack geometries,[90] most probably the role of T atom solvation via water clusters leads to the necessary reduced free energy for framework extraction of aluminum atoms.[91,92] As discussed by Weckhuysen et al., this type of "microsolvation" by multiple water molecules facilitates proton transfer over multiple waters, lowering reaction barriers for framework hydrolysis.[91] As shown by the TGA-MS data above, the presence of a significant amount of "strongly bound" water remaining in the zeolite at elevated temperatures suggests that our results are consistent with the proposed water solvation models.

Effect of Si/Al. A similar liquid water experimental protocol was carried out using HY catalysts having a Si/Al equal to 15 (HY-15), with resulting samples denoted as HY-15-LW. As shown by the quantitative NMR data in Figure S11, the lower-Al-content catalyst proved to be much more stable in excess liquid water at room temperature using the same conditions as for HY-2.6, i.e., 1 h liquid exposure, with the HY-15-LW samples maintaining a total BAS concentration of 0.37 mmol/g that was identical within error to the starting HY-15 catalyst value of 0.34 mmol/g. As an additional verification, IPA-TPD yielded a value for the BAS concentration in the starting HY-15 of 0.37 mmol/g, in complete agreement with the NMR data. Importantly, the typical aqueous ion-exchange procedure used throughout the catalyst literature involves multiple ion-exchange sequences at elevated temperatures of 70−80 °C.[93−95] Even though HY-15 is more stable to the brief liquid water exposure and removal conditions that were shown in Figures 1−6 to degrade the HY-2.6 structure, the data in the top trace of Figure S11 clearly show that HY-15 loses over half of its total Brönsted acid site density using the most commonly employed catalyst modification methods, with final Σ(BAS) = 0.14. To clarify, this triply "exchanged" sample contained no exchangeable cation, only water in each of the three dissolution steps, but the resulting data indicates that the same concerns about correct data interpretation following common catalyst manipulation steps, preservation of acidity and structural integrity, and extension of HY catalysts to aqueous-rich environments must be considered for catalysts with larger Si/Al.

https://doi.org/10.1021/jacs.3c12437
J. Am. Chem. Soc. 2024, 146, 1132−1143

CONCLUSIONS

Detailed spectroscopy, crystallography, and flow-reactor experiments have shown that Brønsted acid site (BAS) density for zeolite HY can decrease by a factor of 10 following exposure to room-temperature liquid water. These data indicate that aqueous-phase ion-exchange procedures commonly used to modify zeolite Y are impacted by the liquid water and primarily by its removal, even when fractional heating rates and inert water removal conditions much less severe than those in standard practice are used for catalyst dehydration. The structural impact of low-temperature ion-exchange methods in liquid water complicates data interpretation from the introduced cations on catalyst performance and likely explains the wide variation in reported acid site concentrations and catalyst activity for zeolite HY with high-Al content. While the ammonium form of the catalyst is largely immune to liquid water exposure and removal, many catalytically important questions involving differential HY acidity for sites in sodalite versus supercages, paired versus isolated sites, synergistic sites, and Brønsted–Lewis pairs require that the proton form of the catalyst be used. The work described here demonstrates any liquid water exposure can significantly decrease the final activity of the catalyst due to the deleterious impacts of removing a strongly bound water fraction in the protonic catalyst form. The differential water-induced impacts on active sites in sodalite vs supercage positions revealed here suggest that controlled modifications of active site locations can be induced using benign water-based chemistries.

ASSOCIATED CONTENT

Supporting Information

The Supporting Information is available free of charge at https://pubs.acs.org/doi/10.1021/jacs.3c12437.

Additional information, including XRD data, TGA-MS data, NMR data, and isooctane reaction data (PDF)

AUTHOR INFORMATION

Corresponding Author

Jeffery L. White − *School of Chemical Engineering, Oklahoma State University, Stillwater, Oklahoma 74078, United States;* orcid.org/0000-0003-4065-321X; Email: jeff.white@okstate.edu

Authors

Anya Zornes − *School of Chemical Engineering, Oklahoma State University, Stillwater, Oklahoma 74078, United States;* orcid.org/0009-0001-8119-2803

Nabihan B. Abdul Rahman − *School of Sustainable Chemical, Biological, and Materials Engineering, University of Oklahoma, Norman, Oklahoma 73019, United States*

Omio Rani Das − *School of Chemical Engineering, Oklahoma State University, Stillwater, Oklahoma 74078, United States*

Laura A. Gomez − *School of Sustainable Chemical, Biological, and Materials Engineering, University of Oklahoma, Norman, Oklahoma 73019, United States*

Steven Crossley − *School of Sustainable Chemical, Biological, and Materials Engineering, University of Oklahoma, Norman, Oklahoma 73019, United States;* orcid.org/0000-0002-1017-9839

Daniel E. Resasco − *School of Sustainable Chemical, Biological, and Materials Engineering, University of Oklahoma, Norman, Oklahoma 73019, United States;* orcid.org/0000-0001-5342-0621

Complete contact information is available at: https://pubs.acs.org/10.1021/jacs.3c12437

Notes

The authors declare no competing financial interest.

ACKNOWLEDGMENTS

The authors are grateful for the support of this work from the National Science Foundation under Grant No. CHE-2154398 and CHE-2154399.

REFERENCES

(1) Corma, A. Inorganic Solid Acids and Their Use in Acid-Catalyzed Hydrocarbon Reactions. *Chem. Rev.* **1995**, *95* (3), 559–614.

(2) Thomas, J. M.; Thomas, W. J. *Principles and Practice of Heterogeneous Catalysis*; VCH: Weinheim, 1996.

(3) Derouane, E. G.; Védrine, J. C.; Pinto, R. R.; Borges, P. M.; Costa, L.; Lemos, M. A. N. D. A.; Lemos, F.; Ribeiro, F. R. The Acidity of Zeolites: Concepts, Measurements and Relation to Catalysis: A Review on Experimental and Theoretical Methods for the Study of Zeolite Acidity. *Catal. Rev.* **2013**, *55* (4), 454–515.

(4) Xiong, H.; Pham, H. N.; Datye, A. K. Hydrothermally stable heterogeneous catalysts for conversion of biorenewables. *Green Chem.* **2014**, *16* (11), 4627–4643.

(5) Huo, J.; Tessonnier, J.-P.; Shanks, B. H. Improving Hydrothermal Stability of Supported Metal Catalysts for Biomass Conversions: A Review. *ACS Catal.* **2021**, *11* (9), 5248–5270.

(6) Huber, G. W.; Chheda, J. F.; Barrett, C. J.; Barrett, C. F.; Dumesic, J. A.; Dumesic, J. A. Production of liquid alkanes by aqueous-phase processing of biomass-derived carbohydrates. *Science* **2005**, *308*, 1446–1450.

(7) Taarning, E.; Osmundsen, C. M.; Yang, X.; Voss, B.; Andersen, S. I.; Christensen, C. H. Zeolite-catalyzed biomass conversion to fuels and chemicals. *Energy Environ. Sci.* **2011**, *4* (3), 793–804.

(8) Dimitrijevic, R.; Lutz, W.; Ritzmann, A. Hydrothermal stability of zeolites: Determination of extra-framework species of H-Y faujasite-type steamed zeolite. *J. Phys. Chem. Solids* **2006**, *67* (8), 1741–1748.

(9) Zhang, L.; Chen, K.; Chen, B.; White, J. L.; Resasco, D. E. Factors that Determine Zeolite Stability in Hot Liquid Water. *J. Am. Chem. Soc.* **2015**, *137* (36), 11810–11819.

(10) Deng, C.; Zhang, J.; Dong, L.; Huang, M.; Bin, L.; Jin, G.; Gao, J.; Zhang, F.; Fan, M.; Zhang, L.; Gong, Y. The effect of positioning cations on acidity and stability of the framework structure of Y zeolite. *Sci. Rep.* **2016**, *6* (1), No. 23382.

(11) Ravenelle, R. M.; Schüßler, F.; D'Amico, A.; Danilina, N.; van Bokhoven, J. A.; Lercher, J. A.; Jones, C. W.; Sievers, C. Stability of Zeolites in Hot Liquid Water. *J. Phys. Chem. C* **2010**, *114* (46), 19582–19595.

(12) Prodinger, S.; Derewinski, M. A.; Vjunov, A.; Burton, S. D.; Arslan, I.; Lercher, J. A. Improving Stability of Zeolites in Aqueous Phase via Selective Removal of Structural Defects. *J. Am. Chem. Soc.* **2016**, *138* (13), 4408–4415.

(13) Wouters, B. H.; Chen, T.; Grobet, P. J. Steaming of Zeolite Y: Formation of Transient Al Species. *J. Phys. Chem. B* **2001**, *105* (6), 1135–1139.

(14) Xu, B.; Bordiga, S.; Prins, R.; van Bokhoven, J. A. Effect of framework Si/Al ratio and extra-framework aluminum on the catalytic activity of Y zeolite. *Appl. Catal., A* **2007**, *333* (2), 245–253.

(15) Du, X.; Gao, X.; Zhang, H.; Li, X.; Liu, P. Effect of cation location on the hydrothermal stability of rare earth-exchanged Y zeolites. *Catal. Commun.* **2013**, *35*, 17–22.

(16) Louwen, J. N.; Simko, S.; Stanciakova, K.; Bulo, R. E.; Weckhuysen, B. M.; Vogt, E. T. C. Role of Rare Earth Ions in the

Prevention of Dealumination of Zeolite Y for Fluid Cracking Catalysts. *J. Phys. Chem. C* **2020**, *124* (8), 4626−4636.
(17) Sanchez-Castillo, M. A.; Madon, R. J.; Dumesic, J. A. Role of Rare Earth Cations in Y Zeolite for Hydrocarbon Cracking. *J. Phys. Chem. B* **2005**, *109* (6), 2164−2175.
(18) Lemos, F.; Ramôa Ribeiro, F.; Kern, M.; Giannetto, G.; Guisnet, M. Influence of lanthanum content of LaHY catalysts on their physico-chemical and catalytic properties: Comparison with CeHY catalysts. *Appl. Catal.* **1988**, *39*, 227−237.
(19) Vu, H.-T.; Harth, F. M.; Wilde, N. Silylated Zeolites With Enhanced Hydrothermal Stability for the Aqueous-Phase Hydrogenation of Levulinic Acid to γ-Valerolactone. *Front. Chem.* **2018**, *6*, No. 143, DOI: 10.3389/fchem.2018.00143.
(20) Prodinger, S.; Derewinski, M. A. Recent Progress to Understand and Improve Zeolite Stability in the Aqueous Medium. *Pet. Chem.* **2020**, *60* (4), 420−436.
(21) Buttersack, C.; König, A.; Gläser, R. Stability of a highly dealuminated Y-zeolite in liquid aqueous media. *Microporous Mesoporous Mater.* **2019**, *281*, 148−160.
(22) Zapata, P. A.; Faria, J.; Ruiz, M. P.; Jentoft, R. E.; Resasco, D. E. Hydrophobic Zeolites for Biofuel Upgrading Reactions at the Liquid−Liquid Interface in Water/Oil Emulsions. *J. Am. Chem. Soc.* **2012**, *134* (20), 8570−8578.
(23) Kuwahara, Y.; Kamegawa, T.; Mori, K.; Matsumura, Y.; Yamashita, H. Fabrication of Hydrophobic Zeolites Using Triethoxyfluorosilane and their Application for Photocatalytic Degradation of Acetaldehyde. *Top. Catal.* **2009**, *52* (6), 643−648.
(24) Di Iorio, J. R.; Gounder, R. Controlling the Isolation and Pairing of Aluminum in Chabazite Zeolites Using Mixtures of Organic and Inorganic Structure-Directing Agents. *Chem. Mater.* **2016**, *28*, 2236−2247.
(25) Pham, T. N.; Nguyen, V.; Nguyen-Phu, H.; Wang, B.; Crossley, S. Influence of Brønsted Acid Site Proximity on Alkane Cracking in MFI Zeolites. *ACS Catal.* **2023**, *13*, 1359−1370.
(26) Chen, K.; Abdolrahmani, M.; Horstmeier, S.; Pham, T. N.; Nguyen, V. T.; Zeets, M.; Wang, B.; Crossley, S.; White, J. L. Brønsted−Brønsted Synergies between Framework and Noncrystalline Protons in Zeolite H-ZSM-5. *ACS Catal.* **2019**, *9* (7), 6124−6136.
(27) Hunger, M.; Freude, D.; Pfeifer, H.; Prager, D.; Reschetilowski, W. Proton MAS NMR studies of hydroxyl groups in alkaline earth cation-exchanged zeolite Y. *Chem. Phys. Lett.* **1989**, *163* (2), 221−224.
(28) Qiu, L.; Ying, F. U.; Jinyu, Z.; Nangui, H.; Lijun, L. U.; Xiuzhi, G. A. O.; Mudi, X. I. N.; Yibin, L. U. O.; Yanqiang, S. H. I.; Guangtong, X. U. Investigation on the cation location, structure and performances of rare earth-exchanged Y zeolite. *J. Rare Earths* **2017**, *35* (7), 658−666.
(29) Lemos, F.; Ribeiro, F. R.; Kern, M.; Giannetto, G.; Guisnet, M. Influence of the cerium content of CeHY catalysts on their physicochemical and catalytic properties. *Appl. Catal.* **1987**, *29* (1), 43−54.
(30) Zu, Y.; Hui, Y.; Qin, Y.; Zhang, L.; Liu, H.; Zhang, X.; Guo, Z.; Song, L.; Gao, X. Facile fabrication of effective Cerium(III) hydroxylated species as adsorption active sites in CeY zeolite adsorbents towards ultra-deep desulfurization. *Chem. Eng. J.* **2019**, *375*, No. 122014.
(31) Pugh, S. M.; Wright, P. A.; Law, D. J.; Thompson, N.; Ashbrook, S. E. Facile, Room-Temperature 17O Enrichment of Zeolite Frameworks Revealed by Solid-State NMR Spectroscopy. *J. Am. Chem. Soc.* **2020**, *142* (2), 900−906.
(32) Brinkmann, A.; Kentgens, A. P. M. Proton-Selective 17O−H Distance Measurements in Fast Magic-Angle-Spinning Solid-State NMR Spectroscopy for the Determination of Hydrogen Bond Lengths. *J. Am. Chem. Soc.* **2006**, *128* (46), 14758−14759.
(33) Peng, L.; Huo, H.; Liu, Y.; Grey, C. P. 17O Magic Angle Spinning NMR Studies of Brønsted Acid Sites in Zeolites HY and HZSM-5. *J. Am. Chem. Soc.* **2007**, *129* (2), 335−346.
(34) Heard, C. J.; Grajciar, L.; Rice, C. M.; Pugh, S. M.; Nachtigall, P.; Ashbrook, S. E.; Morris, R. E. Fast room temperature lability of aluminosilicate zeolites. *Nat. Commun.* **2019**, *10* (1), No. 4690.
(35) Amoureux, J. P.; Bauer, F.; Ernst, H.; Fernandez, C.; Freude, D.; Michel, D.; Pingel, U. T. 17O multiple-quantum and 1H MAS NMR studies of zeolite ZSM-5. *Chem. Phys. Lett.* **1998**, *285* (1), 10−14.
(36) Mezari, B.; Magusin, P. C. M. M.; Almutairi, S. M. T.; Pidko, E. A.; Hensen, E. J. M. Nature of Enhanced Brønsted Acidity Induced by Extraframework Aluminum in an Ultrastabilized Faujasite Zeolite: An In Situ NMR Study. *J. Phys. Chem. C* **2021**, *125* (17), 9050−9059.
(37) Thomas, B.; Ramu, V. G.; Gopinath, S.; George, J.; Kurian, M.; Laurent, G.; Drisko, G. L.; Sugunan, S. Catalytic acetalization of carbonyl compounds over cation (Ce3+, Fe3+ and Al3+) exchanged montmorillonites and Ce3+-exchanged Y zeolites. *Appl. Clay Sci.* **2011**, *53* (2), 227−235.
(38) Altwasser, S.; Jiao, J.; Steuernagel, S.; Weitkamp, J.; Hunger, M. Elucidating the Dealumination Mechanism of Zeolite H-Y by Solid-State NMR Spectroscopy. In *Studies in Surface Science and Catalysis*; van Steen, E.; Claeys, M.; Callanan, L. H., Eds.; Elsevier, 2004; Vol. *154*, pp 1212−1213.
(39) Wang, N.-N.; Wang, Y.; Cheng, H.-F.; Tao, Z.; Wang, J.; Wu, W.-Z. Impact of cationic lanthanum species on zeolite Y: an infrared, excess infrared and Raman spectroscopic study. *RSC Adv.* **2013**, *3* (43), 20237−20245.
(40) Garcia, F. A. C.; Araújo, D. R.; Silva, J. C. M.; Macedo, J. L. d.; Ghesti, G. F.; Dias, S. C. L.; Dias, J. A.; R Filho, G. N. Effect of cerium loading on structure and morphology of modified Ce-USY zeolites. *J. Braz. Chem. Soc.* **2011**, *22*, 1894−1902, DOI: 10.1590/S0103-50532011001000010.
(41) van Bokhoven, J. A.; van der Eerden, A. M. J.; Koningsberger, D. C. Three-Coordinate Aluminum in Zeolites Observed with In situ X-ray Absorption Near-Edge Spectroscopy at the Al K-Edge: Flexibility of Aluminum Coordinations in Zeolites. *J. Am. Chem. Soc.* **2003**, *125* (24), 7435−7442.
(42) Jiao, J.; Wang, W.; Sulikowski, B.; Weitkamp, J.; Hunger, M. 29Si and 27Al MAS NMR characterization of non-hydrated zeolites Y upon adsorption of ammonia. *Microporous Mesoporous Mater.* **2006**, *90* (1), 246−250.
(43) Omegna, A.; van Bokhoven, J. A.; Prins, R. Flexible Aluminum Coordination in Alumino−Silicates. Structure of Zeolite H−USY and Amorphous Silica−Alumina. *J. Phys. Chem. B* **2003**, *107* (34), 8854−8860.
(44) Ravi, M.; Sushkevich, V. L.; van Bokhoven, J. A. On the location of Lewis acidic aluminum in zeolite mordenite and the role of framework-associated aluminum in mediating the switch between Brønsted and Lewis acidity. *Chem. Sci.* **2021**, *12* (11), 4094−4103.
(45) Xu, B.; Rotunno, F.; Bordiga, S.; Prins, R.; van Bokhoven, J. A. Reversibility of structural collapse in zeolite Y: Alkane cracking and characterization. *J. Catal.* **2006**, *241* (1), 66−73.
(46) Wouters, B. H.; Chen, T. H.; Grobet, P. J. Reversible Tetrahedral−Octahedral Framework Aluminum Transformation in Zeolite Y. *J. Am. Chem. Soc.* **1998**, *120* (44), 11419−11425.
(47) Jiao, J.; Altwasser, S.; Wang, W.; Weitkamp, J.; Hunger, M. State of Aluminum in Dealuminated, Nonhydrated Zeolites Y Investigated by Multinuclear Solid-State NMR Spectroscopy. *J. Phys. Chem. B* **2004**, *108* (38), 14305−14310.
(48) Guo, Y.; Jia, H.; Qi, J.; Fan, B.; Qin, B.; Ma, J.; Du, Y.; Li, R. Acid and steric synergies in industrial Y zeolites for 9, 10-dihydroanthracene hydrocracking. *Catal. Commun.* **2023**, *177*, No. 106655.
(49) Corma, A.; Fornés, V.; Melo, F. V.; Herrero, J. Comparison of the information given by ammonia t.p.d. and pyridine adsorption—desorption on the acidity of dealuminated HY and LaHY zeolite cracking catalysts. *Zeolites* **1987**, *7* (6), 559−563.
(50) Almutairi, S. M. T.; Mezari, B.; Pidko, E. A.; Magusin, P. C. M. M.; Hensen, E. J. M. Influence of steaming on the acidity and the methanol conversion reaction of HZSM-5 zeolite. *J. Catal.* **2013**, *307*, 194−203.

(51) To, A. T.; Jentoft, R. E.; Alvarez, W. E.; Crossley, S. P.; Resasco, D. E. Generation of synergistic sites by thermal treatment of HY zeolite. Evidence from the reaction of hexane isomers. *J. Catal.* **2014**, *317*, 11−21.
(52) Wang, X.; Coleman, J.; Jia, X.; White, J. L. Quantitative Investigations of Acidity, and Transient Acidity, in Zeolites and Molecular Sieves. *J. Phys. Chem. B* **2002**, *106* (19), 4941−4946.
(53) Engelhardt, G.; Lohse, U.; Mägi, M.; Lippmaa, E. Solid State 29Si and 27 Al Nmr Studies of Decationized and Dealuminated Zeolites. In *Studies in Surface Science and Catalysis*; Jacobs, P. A.; Jaeger, N. I.; Jírů, P.; Kazansky, V. B.; Schulz-Ekloff, G., Eds.; Elsevier, 1984; Vol. *18*, pp 23−30.
(54) Du, X.; Zhang, H.; Li, X.; Tan, Z.; Liu, H.; Gao, X. Cation location and migration in lanthanum-exchanged NaY zeolite. *Chin. J. Catal.* **2013**, *34* (8), 1599−1607.
(55) Qin, Z.; Cychosz, K. A.; Melinte, G.; El Siblani, H.; Gilson, J.-P.; Thommes, M.; Fernandez, C.; Mintova, S.; Ersen, O.; Valtchev, V. Opening the Cages of Faujasite-Type Zeolite. *J. Am. Chem. Soc.* **2017**, *139* (48), 17273−17276.
(56) Li, X.; Han, H.; Xu, W.; Hwang, S.-J.; Lu, P.; Bhan, A.; Tsapatsis, M. Enhanced Reactivity of Accessible Protons in Sodalite Cages of Faujasite Zeolite. *Angew. Chem., Int. Ed.* **2022**, *61* (5), No. e202111180.
(57) Thomas, B.; Sugunan, S. Influence of residual cations (Na+, K +, and Mg2+) in the alkylation activity of benzene with 1-octene over rare earth metal ion exchanged FAU−Y zeolite. *Microporous Mesoporous Mater.* **2004**, *72* (1), 227−238.
(58) Zhang, Q.; Gao, S.; Yu, J. Metal Sites in Zeolites: Synthesis, Characterization, and Catalysis. *Chem. Rev.* **2023**, *123*, 6039−6106, DOI: 10.1021/acs.chemrev.2c00315.
(59) Abdolrahmani, M.; Chen, K.; White, J. L. Assessment, control, and impact of Brønsted acid site heterogeneity in zeolite HZSM-5. *J. Phys. Chem. C* **2018**, *122* (27), 15520−15528.
(60) Pham, T. N.; Nguyen, V.; Wang, B.; White, J. L.; Crossley, S. Quantifying the Influence of Water on the Mobility of Aluminum Species and Their Effects on Alkane Cracking in Zeolites. *ACS Catal.* **2021**, *11* (12), 6982−6994.
(61) Song, C.; Chu, Y.; Wang, M.; Shi, H.; Zhao, L.; Guo, X.; Yang, W.; Shen, J.; Xue, N.; Peng, L.; Ding, W. Cooperativity of adjacent Brønsted acid sites in MFI zeolite channel leads to enhanced polarization and cracking of alkanes. *J. Catal.* **2017**, *349*, 163−174.
(62) Lónyi, F.; Valyon, J. A TPD and IR study of the surface species formed from ammonia on zeolite H-ZSM-5, H-mordenite and H-beta. *Thermochim. Acta* **2001**, *373* (1), 53−57.
(63) Kerr, G. T. Evidence that Breck and Skeels prepared hydrogen zeolite Y. *J. Catal.* **1982**, *77* (1), 307−308.
(64) Parker, L. M.; Bibby, D. M.; Burns, G. R. Interaction of water with the zeolite HY, studied by FT i.r. *Zeolites* **1991**, *11* (3), 293−297.
(65) Heard, C. J.; Grajciar, L.; Uhlík, F.; Shamzhy, M.; Opanasenko, M.; Čejka, J.; Nachtigall, P. Zeolite (In)Stability under Aqueous or Steaming Conditions. *Adv. Mater.* **2020**, *32* (44), No. 2003264.
(66) Batool, S. R.; Sushkevich, V. L.; van Bokhoven, J. A. Correlating Lewis acid activity to extra-framework aluminum species in zeolite Y introduced by ion-exchange. *J. Catal.* **2022**, *408*, 24−35.
(67) Mitchell, S.; Milina, M.; Verel, R.; Hernández-Rodríguez, M.; Pinar, A. B.; McCusker, L. B.; Pérez-Ramírez, J. Aluminum Redistribution during the Preparation of Hierarchical Zeolites by Desilication. *Chem. - Eur. J.* **2015**, *21* (40), 14156−14164.
(68) Thomas, B.; Ramu, V. G.; Gopinath, S.; George, J.; Kurian, M.; Laurent, G.; Drisko, G. L.; Sugunan, S. Catalytic acetalization of carbonyl compounds over cation (Ce3+, Fe3+ and Al3+) exchanged montmorillonites and Ce3+ exchanged Y zeolites. *Appl. Clay Sci.* **2011**, *53* (2), 227−235.
(69) Hunger, M.; Schenk, U.; Weitkamp, J. Mechanistic studies of the side-chain alkylation of toluene with methanol on basic zeolites Y by multi-nuclear NMR spectroscopy1Dedicated to Professor Herman van Bekkum on the occasion of his 65th birthday.1. *J. Mol. Catal. A: Chem.* **1998**, *134* (1), 97−109.
(70) Gaare, K.; Akporiaye, D. Effects of La Exchange on NaY and NaX Zeolites As Characterized by 29Si NMR. *J. Phys. Chem. B* **1997**, *101* (1), 48−54.
(71) Nery, J. G.; Mascarenhas, Y. P.; Bonagamba, T. J.; Mello, N. C.; Souza-Aguiar, E. F. Location of cerium and lanthanum cations in CeNaY and LaNaY after calcination. *Zeolites* **1997**, *18* (1), 44−49.
(72) Hunger, M.; Engelhardt, G.; Koller, H.; Weitkamp, J. Characterization of sodium cations in dehydrated faujasites and zeolite EMT by 23Na DOR, 2D nutation, and MAS NMR. *Solid State Nucl. Magn. Reson.* **1993**, *2* (3), 111−120.
(73) Mortier, W. J.; Bosmans, H. J. Location of univalent cations in synthetic zeolites of the Y and X type with varying silicon to aluminum ratio. I. Hydrated potassium exchanged forms. *J. Phys. Chem. A* **1971**, *75* (21), 3327−3334.
(74) Jiao, J.; Kanellopoulos, J.; Wang, W.; Ray, S. S.; Foerster, H.; Freude, D.; Hunger, M. Characterization of framework and extra-framework aluminum species in non-hydrated zeolites Y by 27Al spin-echo, high-speed MAS, and MQMAS NMR spectroscopy at B0 = 9.4 to 17.6 T. *Phys. Chem. Chem. Phys.* **2005**, *7* (17), 3221−3226.
(75) Weihe, M.; Hunger, M.; Breuninger, M.; Karge, H. G.; Weitkamp, J. Influence of the Nature of Residual Alkali Cations on the Catalytic Activity of Zeolites X, Y, and EMT in their Brønsted Acid Forms. *J. Catal.* **2001**, *198* (2), 256−265.
(76) Hunger, M.; Horvath, T. Conversion of Propan-2-ol on Zeolites LaNaY and HY Investigated by Gas Chromatography and In-Situ MAS NMR Spectroscopy under Continuous-Flow Conditions. *J. Catal.* **1997**, *167* (1), 187−197.
(77) Klein, H.; Fuess, H.; Hunger, M. Cation location and migration in lanthanum-exchanged zeolite NaY studied by X-ray powder diffraction and MAS NMR spectroscopy. *J. Chem. Soc., Faraday Trans.* **1995**, *91* (12), 1813−1824.
(78) Norby, P.; Poshni, F. I.; Gualtieri, A. F.; Hanson, J. C.; Grey, C. P. Cation Migration in Zeolites: An in Situ Powder Diffraction and MAS NMR Study of the Structure of Zeolite Cs(Na)−Y during Dehydration. *J. Phys. Chem. B* **1998**, *102* (5), 839−856.
(79) Dosen, A.; Marinkovic, B. A. Negative thermal expansion and cationic migration in zeolite Y used in FCC catalysts. *Bull. Mater. Sci.* **2019**, *42* (3), No. 86.
(80) Chen, K.; Kelsey, J.; Zhang, L.; Resasco, D.; White, J. L. Water interactions in zeolite catalysts and their hydrophobically modified analogues. *ACS Catal.* **2015**, *5* (12), 7480−7487.
(81) Wang, M.; Jaeger, N.; Lee, M.; Wan, C.; Hu, J.; Shi, H.; Mei, D.; Burton, S.; Camaioni, D.; Gutirrez, O.; Glezakou, V.; Rousseau, R.; Wang, Y.; Lercher, J. A. Genesis and stability of hydronium ions in zeolite channels. *J. Am. Chem. Soc.* **2019**, *141*, 3444−3445.
(82) Grobet, P. J.; Geerts, H.; Tielen, M.; Martens, J. A.; Jacobs, P. A. Framework and Non-Framework Al Species in Dealuminated Zeolite Y. In *Studies in Surface Science and Catalysis*; Karge, H. G.; Weitkamp, J., Eds.; Elsevier, 1989; Vol. *46*, pp 721−734.
(83) Sanz, J.; Fornés, V.; Corma, A. Extraframework aluminium in steam- and SiCl4-dealuminated Y zeolite. A 27Al and 29Si nuclear magnetic resonance study. *J. Chem. Soc., Faraday Trans. 1* **1988**, *84* (9), 3113−3119.
(84) Ennaert, T.; Geboers, J.; Gobechiya, E.; Courtin, C. M.; Kurttepeli, M.; Houthoofd, K.; Kirschhock, C. E. A.; Magusin, P. C. M. M.; Bals, S.; Jacobs, P. A.; Sels, B. F. Conceptual Frame Rationalizing the Self-Stabilization of H-USY Zeolites in Hot Liquid Water. *ACS Catal.* **2015**, *5* (2), 754−768.
(85) Lippmaa, E.; Samoson, A.; Magi, M. High-resolution aluminum-27 NMR of aluminosilicates. *J. Am. Chem. Soc.* **1986**, *108* (8), 1730−1735.
(86) Brillis, A. A.; Manos, G.Catalyst Deactivation during Catalytic Cracking of N-Octane, Isooctane, and 1-Octene over USHY Zeolite. In *Studies in Surface Science and Catalysis*; Elsevier, 2001; Vol. *139*, p 255.
(87) Brillis, A. A.; Manos, G. Deactivation Studies During Catalytic Cracking of C_8 Aliphatic Hydrocarbons over Ultrastable Y-Zeolite. Conversion and Product Yield Profiles with Time Onstream. *Catal. Lett.* **2003**, *91*, 185.

(88) Chen, K.; Horstmeier, S.; Nguyen, V. T.; Wang, B.; Crossley, S. P.; Pham, T.; Gan, Z.; Hung, I.; White, J. L. Structure and Catalytic Characterization of a Second Framework Al(IV) Site in Zeolite Catalysts Revealed by NMR at 35.2 T. *J. Am. Chem. Soc.* **2020**, *142* (16), 7514−7523.
(89) Grifoni, E.; Piccini, G.; Lercher, J. A.; Glezakou, V.; Rousseau, R.; Parinello, M. Confinement Effects and Acid Strength in Zeolites. *Nat. Commun.* **2021**, *12*, No. 2630.
(90) Silaghi, M.-C.; Chizallet, C.; Sauer, J.; Raybaud, P. Dealumination mechanisms of zeolites and extra-framework aluminum confinement. *J. Catal.* **2016**, *339*, 242−255.
(91) Staciakova, K.; Ensing, B.; Goltl, F.; Bulo, R.; Weckhuysen, B. M. Cooperative Role of Water Molecules during the Initial Stage of Water-Induced Dealumination. *ACS Catal.* **2019**, *9*, 5119−5135.
(92) Resasco, D. E.; Crossley, S. P.; Wang, B.; White, J. L. Interaction of Water with Zeolites: A Review. *Catal. Rev.* **2021**, *63* (2), 302−362.
(93) Carvajal, R.; Chu, P.-J.; Lunsford, J. H. The Role of Polyvalent Cations in Developing Strong Acidity: A Study of Lanthanum-Exchanged Zeolites. *J. Catal.* **1990**, *125* (1), 123−131.
(94) Fritz, P. O.; Lunsford, J. H. The Effect of Sodium Poisoning on Dealuminated Y-Type Zeolites. *J. Catal.* **1989**, *118* (1), 85−98.
(95) Hopfl, V.; Schachtl, T.; Liu, Y.; Lercher, J. A. Pellet Size-Induced Increase in Catalyst Stability and Yield in Zeolite-Catalyzed 2-Butene/Isobutane Aklylation. *Ind. Eng. Chem. Res.* **2022**, *61*, 330−338.

https://doi.org/10.1021/jacs.3c12437
J. Am. Chem. Soc. 2024, 146, 1132−1143